# DENSITY FUNCTIONAL THEORY BASED COMPARATIVE ANALYSIS OF STRUCTURAL AND BIOLOGICAL ACTIVITIES OF THALIDOMIDE AND ITS METHYL DERIVATIVES

*P. NISHAD*, A.K. DWIVEDI**, A. TIWARI*, A.K. PANDEY*, S.N. TIWARI*, G. MISHRA*, D.D. DUBEY*, V. SINGH***, S.I. ANSARI****, V.N. MISHRA****#*

*Department of Physics, "K.S. Saket" P.G. College, Ayodhya (UP), India

**Department of Chemistry, "Kisan" College Sohsarai, Biharsharif Nalanda, Bihar, India

***Department of Physics, College of Natural and Mathematical Sciences, University of Dodoma, Dodoma 259, Tanzania

****Department of Physics, "Shri Ramswaroop" Memorial college of Engineering & Management, Lucknow (UP), India, #e-mail: vnvictorious@gmail.com

https://www.doi.org/10.59277/RJB.2026.2.02

*Abstract*. In present communication geometry optimization vibrational analysis of thalidomide (molecule A) and its methyl isomer (molecule B) has been carried out by density functional theory with the B3LYP hybrid functional and a comprehensive 6-311+G(d,p) basis set. The computed bond length and angle of glutarimide's ring in molecule B are changed due to electron withdrawing methyl group substitution. The vibrational assignments of both molecules A and B are made by using animated Gauss View with high order accuracy. The electronic properties and chemical reactivity descriptor like absolute electronegativity (χ), ionization potential (μ), chemical hardness (η), chemical softness (*S*) of molecules A and B are computed by highest occupied molecular orbital (HOMO) and lowest unoccupied molecular orbital (LUMO). The computed energy gap (HOMO-LUMO) of molecule B is more reactive than molecule A. The Fukui function (FF) of molecules A and B are computed by Mullikan's charge on atoms and quantitatively computed most electrophilic charge center and nucleophilic charge center however molecular electrostatic potential surface qualitatively predict same results. The natural bond orbital analysis highlights a strong stabilizing charge transfer from the nitrogen lone pair to the antibonding pi orbital (Lp(1)N6 → π*(O1-C10))Of the carbonyl group. This interaction provides stabilization energies of 50.60 kcal/mol for thalidomide and 51.02 kcal/mol for its isomer. The biological activities of both molecules A and B are computed by Prediction of Activity Spectra for

Received: January 2026;

in final form April 2026.

ROMANIAN J. BIOPHYS., Vol. 36, No. 2, P. 000–000, BUCHAREST, 2026.

Substances (PASS) online server. The docking of molecules A and B by P2X7 protein are performed by using SWISS dock online server.

*Key word*s: Density functional theory (DFT), HOMO, LUMO, PASS, docking.

## INTRODUCTION

Now a day quantum chemical method is very important tool to determine various hidden aspects of biomolecules [28, 29]. The structural properties of biomolecules by using quantum chemical method by optimized geometry in ground state. The electronic properties, charge transport properties, active cites by Fukui function (FF) spectral analysis and absorption spectra (UV) are also determined on optimized geometry [38, 51]. The biological properties of biomolecule are also computed by using quantum chemical method. The chemical formula for thalidomide is C13H10N2O4. The artificial derivative of glutamic acid is termed as thalidomide. Thalidomide having ring structure with an asymmetric carbon in the glutarimide ring. The R-thalidomide is the bioactive form of the molecule due to the carbon of the glutarimide ring bonded to the phthalimide bonded by substituent acidic hydrogen at the chiral center [9, 24, 45].

Thalidomide is an oral managed medication utilized to treat numerous cancers such as myeloma, capillary hemangiomas, renal cell carcinoma or gliobastoma and many skin disorders such as erythema nodosum leprosum (ENL), actinic prurigo (AP) and discoid lupus erythematosus (DLE). Thalidomide having some side effects *e.g*. sleepiness, rash, dizziness, tumor lysis syndrome, blood clots, and peripheral neuropathy [49]. Thalidomide is termed as human teratogen and illustrations very serious birth defects if accomplished throughout pregnancy [49]. It causes skeletal deformities such as amelia, absence of bones, and phocomelia. Thalidomide is enough to cause teratogenic effects [4]. The thalidomide drug with calming effects first introduce for pharmacological actions was published in 1956 and marketed in 1957 in West Germany [23, 25]. Thalidomide was sponsored for anxiety, trouble sleeping and morning sickness [27]. In 1961, it had removed from market after thalidomide was found to cause birth defects [50].

In the United States, thalidomide was approved for treatment for cancer in 1998 [42, 47, 48]. Thalidomide has several adverse cardiovascular effects, including risk of heart attacks, pulmonary hypertension, and changes in heart rhythm such as syncope, bradycardia, and atrioventricular block. Other adverse are reported by thalidomide drug like lung inflammation, vomiting, dry mouth, rashes, dry skin, fever, weakness, and a sense of unwellness [19].

Another methyl derivative of thalidomide in the synthesis of the anticonvulsant drugs carbamazepine and oxcarbazepine as well as antidepressant drugs imipramine and desipramine with chemical formula, $C_{14}H_{12}N_2O_4$ [3]. In present communication a comparative analysis of structural, vibrational, electronic, Fukui function (FF), NBO analysis, pharmaceutical properties, and docking study of bioactive molecules thalidomide and its methyl isomer by using density functional theory. Our study provides new chemical active cites of molecule A which helps to open new pharmaceutical cites of both molecules. We hope our study provides new pathways for further research on molecules A and B.

## COMPUTATIONAL DETAILS

Initial geometry was generated from the standard geometrical parameters and was minimized without any constraint in the potential energy surface. The gradient corrected density functional theory with the three-parameter hybrid functional (B3) [22] for the exchange part and the Lee-Yang-Parr (LYP) correlation function [13] has been employed for the computation of molecular structure, vibrational frequencies, HOMO-LUMO, and energies of the optimized structures, using GAUSSIAN 09 [10]. The calculated vibrational frequencies have also been scaled by a factor of 0.963 [12]. By combining the results of the GAUSSVIEW's program [2] with symmetry considerations, vibrational frequency assignments were made with a high degree of accuracy. The prediction of IR frequencies of title compound has been found to be very straightforward using this approach. Density functional theory calculations are reported to provide excellent vibrational frequencies of organic compound if the calculated frequencies are scaled to compensate for the approximate treatment of electron correlation, for basis set deficiencies and for anharmonicity. Several studies have been carried out regarding calculations of vibrational spectra by using B3LYP methods with 6-311+G(d,p) basis set. The scaling factor (0.963) was applied successfully for B3LYP method and was found to be easily transferable in a number of molecules [18]. Thus, vibrational frequencies calculated by using the B3LYP functional with as basis set, can be utilized to eliminate the uncertainties in the fundamental assignment in the IR spectra.

## GEOMETRY OPTIMIZATION

The optimized geometry of molecule A and molecule B are shown in Figure 1, by using DFT/6-311+G(d,p) method. Both molecules, A and B, are unsymmetrical, so C1 point group symmetry. The computed energies optimized geometries of molecules A and B are 911.67 a.u. and −951.44 a.u. The optimized

geometry of molecule A (thalidomide) having phthalimide ring and a connected alpha (3') carbon of glutarimide ring with nitrogen phthalimide's ring however one methyl group ($-CH_3$) has substituted on alpha (3') carbon of glutarimide ring in molecule B attached at meaning it exists as non-superimposable mirror images (enantiomers). The computed bond length of CH in substituted methyl group lies within range (0.99 Å–1.02 Å). In methyl group two CH bond lies in same plane are lies slightly shorter (0.003Å) than other CH bond lies out of plane. The substitution of $-CH_3$ group on glutarimide ring in molecule B creates angular distortion in attached ring which decreases iso angle however increase meta-angle. The iso angle of in glutarimide ring <C10-C7-C8 is 111.58º in molecule A however corresponding angle in molecule B is 112.37º and meta-angle <C8-C9-C14 is 112.34º in molecule A and corresponding angle in molecule B is 112.29º. The average bond length C–C in glutarimide ring is 1.51–1.54 Å in molecule A and corresponding bond length is 1.51 Å–1.55 Å in molecule B. The computed bond length NH and C=O in ring R3 are 1.02 Å and 1.208–1.209 Å respectively in molecule A and corresponding bond length of NH and CO are 1.01 Å and 1.207 Å – 1.208 Å respectively in molecule B. The connected bond length N–C alpha (3') of molecule A is 1.45 Å which increases after substitution of methyl group 1.47 Å. All other geometrical parameters in phthalimide's ring in both A and B are nearly unchanged.

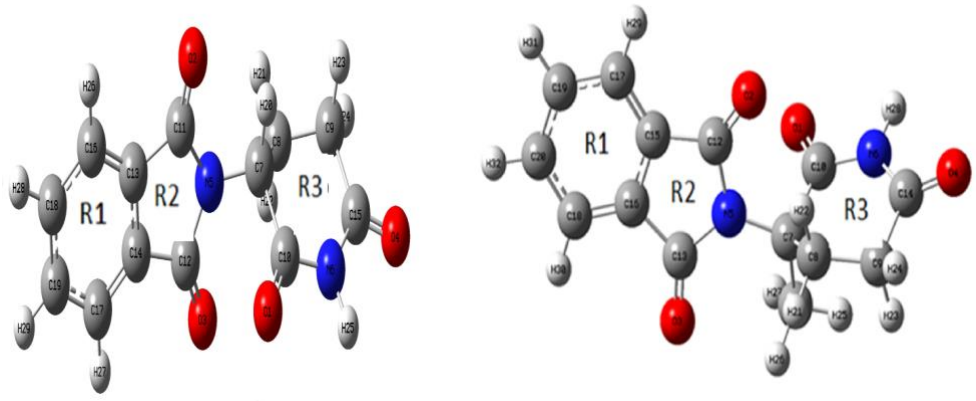


Fig. 1. Optimized geometry of molecules A (Left ) and B (Right).

## ELECTRONIC PROPERTIES

The chemical reactivity or chemical stability is determined by frontier molecular (FMO). In FMO, HOMO is highest occupied molecular orbital, and

LUMO is lowest unoccupied molecular orbital. The supplied energy to transition of electron from HOMO to LUMO is known as energy band gap. The energy gap is directly related with chemical stability[15, 36]. The HOMO represents the ability to donate an electron while LUMO as an electron acceptor and their energies are calculated by DFT/B3LYP method. The electronic parameters, such as highest occupied molecular orbital (HOMO) energy ($E_{HOMO}$), lowest unoccupied molecular orbital (LUMO) energy ($E_{LUMO}$) and band gap energy ($\Delta E = E_{LUMO} - E_{HOMO}$) are described theoretically.

*Table 1*

Several electronic reactivity parameters of molecules A and B by using HOMO & LUMO energy

| **Molecule** | $E_{HOMO}$ (eV) | $E_{LUMO}$ (eV) | $\Delta E_{gap}$ (eV) | **Electro-negativity** ($\chi$) (eV) | **Chemical potential** ($\mu$) (eV) | **Hardness** ($\eta$) (eV) | **Softness** ($S$) $(eV)^{-1}$ | **Electro-philicity** ($\omega$) (eV) |
|---|---|---|---|---|---|---|---|---|
| **A** | –7.673 | –2.775 | 4.898 | 5.226 | –5.226 | 2.446 | 0.204 | 5.583 |
| **B** | –7.565 | –2.748 | 4.817 | 5.160 | –5.160 | 2.415 | 0.207 | 5.511 |

In the present study, the energy ($E_{gap}$) between HOMO and LUMO in the molecule A is found to be 4.898 eV whereas the energy ($E_{gap}$) between HOMO and LUMO in molecule B is 4.817 eV which is lower than corresponding value of molecule A. The computed HOMO and LUMO gap shows that molecule B is more reactive than molecule A. The substitution of methyl group (–CH3) withdrawn charge from glutarimide ring originate more polarity which reduces HOMO and LUMO gap of molecule B. The HOMO and LUMO plot of both molecules A and B are shown in Figure 2.

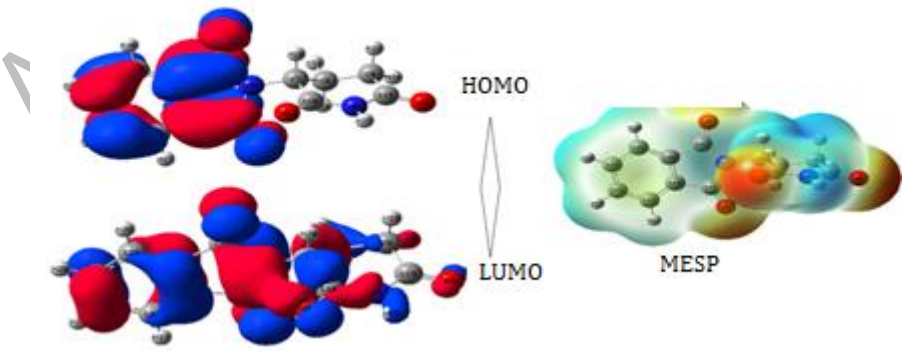

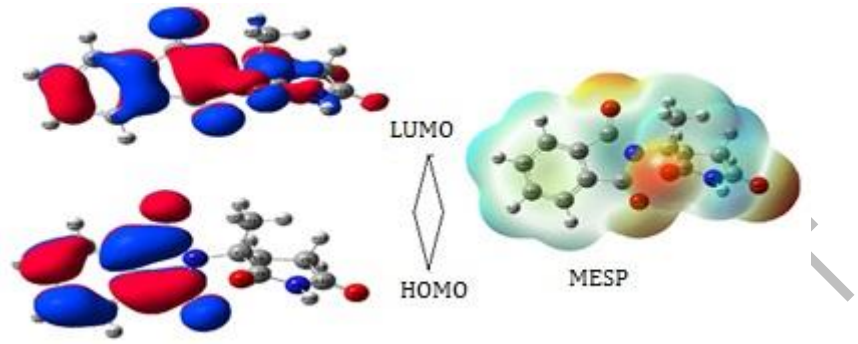


Fig. 2. HOMO, LUMO and MESP plot of molecule A (upper), and molecule B (lower).

The HOMO of both molecules A and B are distributed over whole molecule, however LUMO in both molecules A and B are distributed over whole molecule except glutarimide ring. The HOMO primary acts donor however LUMO acts acceptor so transition of HOMO to LUMO is shows that charge transfer from phthalimide ring to glutarimide ring.

## HOMO-LUMO SURFACE DESCRIPTION

The molecular electrostatic potential (MESP) is a map of potential, *i.e.* electrostatic potential over constant electron density of all molecules. It displays molecular size and shape as well as positive, negative, and neutral electrostatic potential regions in terms of color grading scheme. In this color grading schemes, the blue color represents the most electropositivity *i.e*. low electron region, where as the red color corresponds to the most electronegative center or electron rich regions [14, 30]. The blue color encircled over C8-C9 bond, nitrogen of NH group of glutarimide ring in both molecules A and B however $-CH_3$ group also coded by blue color in molecule B. So, these are electropositive charge center. The nitrogen of phthalimide's ring also coded with blue color in both molecule A and B so this is also electropositive charge center. The red color encircled over both oxygen atoms in glutarimide ring in both molecules A and B.

The energies of frontier molecular orbitals ($E_{\mathrm{HOMO}}$, $E_{\mathrm{LUMO}}$), energy band gap ($E_{\mathrm{LUMO}} - E_{\mathrm{HOMO}}$), electronegativity ($\chi$), chemical potential ($\mu$), global hardness ($\eta$), global softness ($S$), and global electrophilicity index ($\omega$) of have been listed in Table 2. Based on $E_{\mathrm{HOMO}}$ and $E_{\mathrm{LUMO}}$, these parameters are calculated using (1) as given below [5, 16, 31, 32]

$$\chi = -\frac{1}{2}(E_{LUMO} + E_{HOMO}) \quad (1)$$

$$\mu = -\chi = \frac{1}{2}(E_{LUMO} + E_{HOMO}) \quad (2)$$

$$\eta = \frac{1}{2}(E_{LUMO} - E_{HOMO}) \quad (3)$$

$$S = \frac{1}{2\eta} \quad (4)$$

$$\omega = \frac{\mu^2}{2\eta} \quad (5)$$

FUKUI FUNCTION

The Fukui function (FF) [40, 51] of a molecule provides information about reactive site and the method of understanding as well as categorizing chemical reactions. The atom with the highest FF value is highly reactive site as compared to the other atoms in the molecule. The use of the Fukui functions for the site selectivity in title molecule for nucleophilic and electrophilic attacks has been made with special emphasis on the dependence of the Fukui values with the basis of B3LYP/6-311+G(d,p) level of theory. Using the Mullikan's atomic charges of neutral, cation, and anion, state of title molecule, the Fukui functions ($f_k^+$, $f_k^-$, $f_k^0$), local softness ($s_k^+$, $s_k^-$, $s_k^0$) [34] and local electrophilicity indices ($\omega_k^+$, $\omega_k^-$, $\omega_k^0$) are calculated using the following

$$f_k^+ = [(N + 1) - (N)] \text{ for nucleophilic attack} \quad (6)$$

$$f_k^- = [(N) - (N-1)] \text{ for electrophilic attack} \quad (7)$$

$$f_k^0 = 1/2[q\ (N+1) + (N-1)] \text{ for radical attack} \quad (8)$$

Local softness and electrophilicity indices are calculated by using following equations:

$$s_k^{\pm} = S f_k^{\pm} \quad (9)$$

$$s_k^{o} = S f_k^{o} \quad (10)$$

$$\omega_k^{\pm} = \omega f_k^{\pm} \quad (11)$$

$$\omega_k^{o} = \omega f_k^{o} \quad (12)$$

where +, −, and 0 signs show nucleophilic, electrophilic, and radical attack, respectively.

From the Table 2 and Table 3, it can be seen that $O_4$ is the most reactive site for nucleophilic attack in the molecule A and $C_{12}$ is most reactive site in its molecule

B for the nucleophilic attack. For the electrophilic attack, $C_{16}$ is the most reactive site in the title molecule whereas in its conformer, $C_{15}$ is the most reactive site for the electrophilic attack. The most radical site in the conformer is $C_{13}$ whereas in its conformer, $C_{15}$ is the most radical site.

*Table 2*

Computed Fukui function by using Mullikan's atomic charges of neutral, cation, and anion of molecule A

| Atoms | $f_k^+$ | $f_k^-$ | $f_k^0$ | $Sf_k^+$ (eV) | $Sf_k^-$ (eV) | $Sf_k^0$ (eV) | $\omega f_k^+$ $(eV)^{-1}$ | $\omega f_k^-$ $(eV)^{-1}$ | $\omega f_k^0$ $(eV)^{-1}$ |
|---|---|---|---|---|---|---|---|---|---|
| $O_1$ | 0.11466 | 0.01001 | –0.00023 | 0.02344 | 0.00205 | –0.00005 | 0.64014 | 0.05591 | –0.00131 |
| $O_2$ | 0.06191 | 0.14108 | –0.00585 | 0.01265 | 0.02884 | –0.0012 | 0.34562 | 0.78766 | –0.03266 |
| $O_3$ | 0.05380 | 0.13806 | 0.01291 | 0.01100 | 0.02822 | 0.00264 | 0.30037 | 0.77079 | 0.07206 |
| $O_4$ | 0.14431 | 0.04082 | 0.02387 | 0.02950 | 0.00834 | 0.00488 | 0.80569 | 0.22790 | 0.13328 |
| $N_5$ | 0.05416 | –0.0171 | 0.35257 | 0.01107 | –0.00350 | 0.07207 | 0.30237 | –0.09548 | 1.96843 |
| $N_6$ | 0.06060 | 0.02345 | 0.11967 | 0.01239 | 0.00479 | 0.02446 | 0.33835 | 0.13093 | 0.66814 |
| $C_7$ | –0.00146 | 0.06295 | –0.28480 | –0.00030 | 0.01287 | –0.05822 | –0.00813 | 0.35147 | –1.59004 |
| $C_8$ | 0.05249 | –0.01331 | 0.32231 | 0.01073 | –0.00272 | 0.06589 | 0.29304 | –0.07429 | 1.79947 |
| $C_9$ | 0.04524 | 0.01755 | 0.10159 | 0.00925 | 0.00359 | 0.02077 | 0.25257 | 0.09801 | 0.56721 |
| $C_{10}$ | 0.00891 | 0.00663 | 0.15762 | 0.00182 | 0.00136 | 0.03222 | 0.04975 | 0.03701 | 0.87999 |
| $C_{11}$ | 0.01512 | 0.09447 | –0.03501 | 0.00309 | 0.01931 | –0.00716 | 0.08445 | 0.52741 | –0.19548 |
| $C_{12}$ | 0.05007 | 0.08085 | -0.24848 | 0.01024 | 0.01653 | –0.05079 | 0.27953 | 0.45136 | –1.38729 |
| $C_{13}$ | –0.00953 | –0.03286 | 0.48751 | –0.00195 | –0.00672 | 0.09966 | –0.05320 | –0.18345 | 2.72179 |
| $C_{14}$ | –0.00863 | –0.06306 | 0.47793 | –0.00176 | –0.01289 | 0.09770 | –0.04817 | –0.35208 | 2.66829 |
| $C_{15}$ | 0.04245 | 0.01237 | 0.02310 | 0.00868 | 0.00232 | 0.00472 | 0.23698 | 0.06907 | 0.12894 |
| $C_{16}$ | 0.07238 | 0.14574 | –0.01036 | 0.01480 | 0.02979 | –0.00212 | 0.40412 | 0.81366 | –0.05786 |
| $C_{17}$ | 0.07482 | 0.14538 | –0.07293 | 0.01530 | 0.02972 | –0.01491 | 0.41772 | 0.81167 | –0.40719 |

| | | | | | | | | | |
|---|---|---|---|---|---|---|---|---|---|
| $C_{18}$ | 0.08464 | 0.09991 | 0.05728 | 0.01730 | 0.02042 | 0.01171 | 0.47256 | 0.55782 | 0.31982 |
| $C_{19}$ | 0.08405 | 0.10706 | 0.02131 | 0.01718 | 0.02189 | 0.00436 | 0.46928 | 0.59775 | 0.11899 |

*Table 3*

Computed Fukui function by using Mullikan's atomic charges of neutral, cation, and anion of molecule B

| Atoms | $f_k^+$ | $f_k^-$ | $f_k^0$ | $Sf_k^+$ (eV) | $Sf_k^-$ (eV) | $Sf_k^0$ (eV) | $\omega f_k^+$ $(eV)^{-1}$ | $\omega f_k^-$ $(eV)^{-1}$ | $\omega f_k^0$ $(eV)^{-1}$ |
|---|---|---|---|---|---|---|---|---|---|
| $O_1$ | 0.12488 | 0.01495 | 0.02010 | 0.70337 | 0.08422 | 0.11320 | 0.02530 | 0.00303 | 0.00407 |
| $O_2$ | 0.08108 | 0.10123 | 0.03897 | 0.45666 | 0.57018 | 0.21951 | 0.01642 | 0.02050 | 0.00789 |
| $O_3$ | 0.04838 | 0.15624 | 0.01028 | 0.27250 | 0.88000 | 0.05791 | 0.00980 | 0.03164 | 0.00208 |
| $O_4$ | 0.14402 | 0.03958 | 0.02507 | 0.81121 | 0.22295 | 0.14121 | 0.02917 | 0.00802 | 0.00508 |
| $N_5$ | 0.02979 | –0.01124 | 0.38090 | 0.16782 | –0.06332 | 2.14542 | 0.00604 | –0.00228 | 0.07715 |
| $N_6$ | 0.03956 | 0.05229 | 0.11633 | 0.22284 | 0.29450 | 0.65522 | 0.00801 | 0.01059 | 0.02356 |
| $C_7$ | –0.15586 | –0.11042 | –0.41193 | –0.87789 | –0.62195 | –2.32022 | –0.03157 | –0.02236 | –0.08343 |
| $C_8$ | 0.127421 | –0.00158 | 0.44157 | 0.71770 | –0.00892 | 2.48714 | 0.02581 | –0.00032 | 0.08944 |
| $C_9$ | 0.00085 | 0.05374 | 0.05782 | 0.00479 | 0.30272 | 0.32565 | 0.00017 | 0.01089 | 0.01171 |
| $C_{10}$ | –0.15706 | 0.18709 | 0.09965 | –0.88463 | 1.05380 | 0.56128 | –0.03181 | 0.03789 | 0.02018 |
| $C_{11}$ | 0.164148 | 0.09386 | 0.19243 | 0.92457 | 0.52869 | 1.08385 | 0.03325 | 0.01901 | 0.03898 |
| $C_{12}$ | 0.29959 | –0.27169 | –0.40182 | 1.68746 | –1.53031 | –2.26327 | 0.06068 | –0.05503 | –0.08139 |
| $C_{13}$ | –0.05003 | 0.12639 | –0.30133 | –0.28179 | 0.71189 | –1.69726 | –0.01013 | 0.02560 | –0.06103 |
| $C_{14}$ | 0.07343 | –0.02983 | 0.04400 | 0.41359 | –0.16800 | 0.24784 | 0.01487 | –0.00604 | 0.00891 |
| $C_{15}$ | –0.27216 | 0.36410 | 0.68350 | –1.53294 | 2.05082 | 3.84986 | –0.05512 | 0.07375 | 0.13844 |
| $C_{16}$ | 0.14347 | –0.10435 | 0.58008 | 0.80810 | –0.58777 | 3.26733 | 0.02906 | –0.02114 | 0.11749 |
| $C_{17}$ | 0.20138 | –0.02097 | –0.04766 | 1.13425 | –0.11811 | –0.26844 | 0.04079 | –0.00425 | –0.00965 |

| | | | | | | | | | |
|---|---|---|---|---|---|---|---|---|---|
| $C_{18}$ | –0.00536 | 0.17930 | –0.09487 | –0.03020 | 1.00988 | –0.53436 | –0.00109 | 0.03632 | –0.01922 |
| $C_{19}$ | 0.05823 | 0.10985 | 0.02216 | 0.32796 | 0.61871 | 0.12481 | 0.01179 | 0.02225 | 0.00449 |
| $C_{20}$ | 0.10424 | 0.07147 | 0.04476 | 0.58715 | 0.40256 | 0.25210 | 0.02111 | 0.01448 | 0.00906 |

## VIBRATIONAL ANALYSIS

The molecule A and B contain 29 and 32 atoms respectively, so there will be 3N-5 modes of vibration. The molecule A having 82 modes and B contains 91 modes of vibration. Whole spectra of molecule A and B divided in two parts <1000 $cm^{-1}$ are called functional group region, and >1000 $cm^{-1}$ are called fingerprint region. In general, stretching symmetric, antisymmetric, rocking, scissoring modes, in plane bending modes are lies higher frequencies of spectra and out of plane bending, wagging, twisting modes lies lower frequencies region of spectra. Intensity of IR spectra more dependent on polarity amplitude of involved atoms during vibration etc. The computed IR spectra of molecules A and B are shown in Figure 3. Molecules A and B contain no negative frequencies so both molecules are stable. The molecule A and B having –CH, –C=O, methylene (=$CH_2$) and methyl (–$CH_3$) group, –NH functional groups, so we have discussed below.

### N–H vibrational mode

In general, the N–H stretching frequency characteristically seems in the range of 3300–3500 $cm^{-1}$ for non-hydrogen-bonded [7]. In present study, the N–H group present in molecules A and B. In molecule A a significant intense peak appears at 3417 $cm^{-1}$ and their corresponding peak 3415 $cm^{-1}$ in molecule A, which is due to the N–H stretching mode. The N–H in-plane bending mode appears at 1373 $cm^{-1}$ and out of plane bending mode appears at 712 $cm^{-1}$ in molecule A, while corresponding mode appears at 1376 $cm^{-1}$ and 680 $cm^{-1}$ in its molecule B respectively.

In lower frequency regions, some N–H bending mode of vibration along with mixing of other mode of vibration appears in both molecules. The N–H in-plane bending mode appears at 1711 $cm^{-1}$ in the molecule A, while corresponding mode appears at 1707 $cm^{-1}$ molecules A and B along with mixing of several other modes. The variation of N–H in-plane bending mode shows 3–4 $cm^{-1}$ in between molecules A and B. In lower frequency region some significant intense mode appears at 734 $cm^{-1}$, 512 $cm^{-1}$ in molecule A due to the N–H out of plane bending along with mixing of several other bonds and their corresponding mode in molecule B appears at 862 $cm^{-1}$, 548 $cm^{-1}$ respectively.

**C–H vibrational mode**

In general, the C–H stretching vibrations appear in the region of 3300–2800 $cm^{-1}$, which varies on the hybridization of the carbon atom and functional group attached to it [37]. In present study, the C–H group is present in both molecules. The significant intense peak due to C–H stretching mode appears at 3073 $cm^{-1}$, 3059 $cm^{-1}$ in molecule A and their corresponding peak superimpose in its molecule B.

*Table 4*
Vibrational analysis of molecule A

| S.N. | Calculated wavenumber ($cm^{-1}$) | Scaled wavenumber ($cm^{-1}$) | Infrared intensity (a.u.) | Assignment |
|---|---|---|---|---|
| 1 | 466 | 447 | 32 | R ($H_{23}$-$C_9$-$H_{24}$)+ρ (R3) |
| 2 | 566 | 543 | 25 | R ($H_{23}$-$C_9$-$H_{24}$) + γ ($C_{15}$-$O_4$, $N_6$-$H_{25}$) + ρ (R1) |
| 3 | 612 | 588 | 35 | ρ (R2) + R ($H_{23}$-$C_9$-$H_{24}$) + β ($N_6$-$H_{25}$, $C_{10}$-$O_1$) |
| 4 | 732 | 702 | 84 | γ ($C_{16}$-$H_{26}$, $C_{18}$-$H_{28}$, $C_{19}$-$H_{29}$, $C_{17}$-$H_{27}$, $O_2$-$C_{11}$, $O_3$-$C_{12}$) |
| 5 | 742 | 712 | 43 | γ ($N_6$-$H_{25}$) |
| 6 | 764 | 734 | 31 | R ($H_{21}$-$C_8$-$H_{22}$) + γ ($N_6$-$H_{25}$) + ρ (R3) |
| 7 | 900 | 864 | 23 | β ($C_{11}$-$O_2$, $C_{12}$-$O_3$) + β [R1(C-C-C)] + R ($H_{23}$-$C_9$-$H_{24}$) + τ ($H_{21}$-$C_8$-$H_{22}$) |
| 8 | 1018 | 978 | 24 | ρ (R1) + υ ($C_7$-$N_5$, $C_{12}$-$N_5$) + β ($C_7$-$H_{20}$) |
| 9 | 1130 | 1084 | 47 | υ ($C_{11}$-$N_5$, $C_{12}$ - $N_5$) + β ($C_7$-$H_{20}$, $C_8$-$H_{22}$) + τ ($H_{23}$-$C_9$-$H_{24}$) |
| 10 | 1198 | 1150 | 74 | τ ($H_{21}$-$C_8$-$H_{22}$) + γ ($C_7$-$H_{20}$, $C_9$-$H_{23}$) |
| 11 | 1206 | 1158 | 277 | υ ($C_{10}$-$N_6$, $C_{15}$-$N_6$) + τ ($H_{23}$-$C_9$-$H_{24}$) + ω ($H_{21}$-$C_8$-$H_{22}$) |
| 12 | 1276 | 1225 | 136 | τ ($H_{23}$-$C_9$-$H_{24}$) + γ ($C_7$-$H_{20}$) + υ ($C_{10}$-$N_6$) |
| 13 | 1321 | 1268 | 45 | ω ($H_{23}$-$C_9$-$H_{24}$) + γ ($C_7$-$H_{20}$) + υ ($C_{10}$-$N_6$, $C_{15}$-$N_6$) |
| 14 | 1349 | 1295 | 88 | γ ($C_7$-$H_{20}$, $C_8$-$H_{21}$) |
| 15 | 1361 | 1307 | 46 | ω ($H_{23}$-$C_9$-$H_{24}$) + τ ($H_{21}$-$C_8$-$H_{22}$) |
| 16 | 1379 | 1324 | 101 | υ [R1 (C-C-C)] + ρ (R2) + υ ($N_5$-$C_7$) |
| 17 | 1398 | 1342 | 380 | υ ($N_5$-$C_7$, $N_5$-$C_{11}$, $N_5$-$C_{12}$) + υ [R1 (C-C-C)] |
| 18 | 1430 | 1373 | 52 | β ($N_6$-$H_{25}$) |
| 19 | 1773 | 1702 | 719 | υ ($C_{11}$-$O_2$, $C_{12}$-$O_3$) |

| | | | | |
|---|---|---|---|---|
| 20 | 1782 | 1711 | 647 | υ ($C_{10}$-$O_1$, $C_{15}$-$O_4$) + β ($N_6$-$H_{25}$) |
| 21 | 1795 | 1723 | 142 | υ ($C_{10}$-$O_1$, $C_{15}$-$O_4$) |
| 22 | 1827 | 1754 | 72 | υ ($C_{11}$-$O_2$ & $C_{12}$-$O_3$) |
| 23 | 3560 | 3417 | 54 | υ ($N_6$-$H_{25}$) |
| 24 | 3104 | 2979 | 5 | $\upsilon_{as}$ ($H_{21}$-$C_8$-$H_{22}$) |
| 25 | 3186 | 3059 | 5 | υ ($C_{16}$-$H_{26}$, $C_{18}$-$H_{28}$, $C_{19}$-$H_{29}$, $C_{17}$-$H_{27}$) |
| 26 | 3201 | 3073 | 9 | υ ($C_{16}$-$H_{26}$, $C_{18}$-$H_{28}$, $C_{19}$-$H_{29}$, $C_{17}$-$H_{27}$) |
| 27 | 3559 | 3413 | 55 | υ ($N_6$-$H_{28}$) |

*Table 5*

Vibrational analysis of molecule B

| S.N. | Calculated wavenumber ($cm^{-1}$) | Scaled wavenumber ($cm^{-1}$) | Infrared intensity (a.u.) | Assignment |
|---|---|---|---|---|
| 1 | 369 | 354 | 19 | β ($C_{13}$-$O_3$, $C_{12}$-$O_2$) |
| 2 | 399 | 383 | 16 | β ($C_{14}$-$O_4$, $C_{10}$-$O_1$) |
| 3 | 571 | 548 | 19 | R ($H_{23}$-$C_9$-$H_{24}$) + γ ($N_6$-$H_{28}$) |
| 4 | 608 | 584 | 38 | β ($C_{10}$-$O_1$, $C_{14}$-$O_4$, $N_6$-$H_{28}$) + ρ [R2, R3] |
| 5 | 708 | 680 | 22 | γ ($N_6$-$H_{28}$) |
| 6 | 731 | 701 | 73 | γ ($N_5$-$C_{12}$, $N_5$-$C_{13}$, $C_{18}$-$H_{30}$, $C_{20}$-$H_{32}$, $C_{19}$-$H_{31}$, $C_{17}$-$H_{23}$) |
| 7 | 766 | 735 | 56 | γ ($N_6$-$H_{28}$) + R ($H_{21}$-$C_8$-$H_{22}$) |
| 8 | 773 | 742 | 21 | γ ($N_6$-$H_{28}$, $O_1$-$C_{10}$) + R ($H_{21}$-$C_8$-$H_{22}$, $C_{11}$-$H_{25,26,27}$) |
| 9 | 898 | 862 | 20 | β ($N_6$-$H_{28}$, $C_8$-$H_{21}$) + υ [R3(C-C-C)] + ω ($C_{11}$-$H_{25,26,27}$) |
| 10 | 1070 | 1027 | 69 | υ ($N_5$-$C_{12}$, $N_5$-$C_{13}$) + R ($H_{21}$-$C_8$-$H_{22}$, $H_{23}$-$C_9$-$H_{24}$) + R ($C_{11}$-$H_{25,26,27}$) |
| 11 | 1171 | 1124 | 37 | τ($H_{21}$-$C_8$-$H_{22}$) + β($C_{17}$-$H_{29}$, $C_{19}$-$H_{31}$, $C_{20}$-$H_{32}$, $C_{18}$-$H_{30}$) + R($C_{11}$-$H_{25,26,27}$) |
| 12 | 1210 | 1162 | 332 | τ ($H_{23}$-$C_9$-$H_{24}$) + β ($C_8$-$H_{21}$, $N_6$-$H_{28}$) + υ ($N_6$-$C_{10}$, $N_6$-$C_{14}$) |
| 13 | 1228 | 1178 | 34 | ρ (R1) + β ($C_{18}$-$H_{30}$) + υ ($N_5$-$C_7$) + R ($C_{11}$-$H_{25,26,27}$) |
| 14 | 1249 | 1199 | 56 | τ ($H_{23}$-$C_9$-$H_{24}$ + $H_{21}$-$C_8$-$H_{22}$) |
| 15 | 1308 | 1255 | 58 | ω ($H_{23}$-$C_9$-$H_{24}$) + β ($N_6$-$H_{28}$) + τ ($H_{21}$-$C_8$-$H_{22}$) |
| 16 | 1341 | 1288 | 170 | τ ($H_{21}$-$C_8$-$H_{22}$) + υ ($C_7$-$C_{10}$, $N_6$-$C_{10}$, $N_6$-$C_{14}$, $C_9$-$C_{14}$) + ω ($H_{21}$-$C_8$-$H_{22}$) |
| 17 | 1351 | 1297 | 370 | υ ($N_5$-$C_7$, $N_5$-$C_{12}$, $N_5$-$C_{13}$) + υ [R1 (C-C-C)] |
| 18 | 1365 | 1311 | 34 | τ ($H_{21}$-$C_8$-$H_{22}$) + ω ($H_{23}$-$C_9$-$H_{24}$) |

| | | | | |
|---|---|---|---|---|
| 19 | 1385 | 1329 | 17 | ω ($H_{21}$-$C_8$-$H_{22}$) + τ ($H_{23}$-$C_9$-$H_{24}$) |
| 20 | 1392 | 1336 | 103 | υ [R1 (C-C-C), R2 (C-C-C)] + β ($C_{19}$-$H_{31}$, $C_{20}$-$H_{32}$) + ω ($H_{21}$-$C_8$-$H_{22}$) |
| 21 | 1433 | 1376 | 52 | β ($N_6$-$H_{28}$) |
| 22 | 1486 | 1426 | 15 | χ ($H_{26}$-$C_{11}$-$H_{25}$, $H_{26}$-$C_{11}$-$H_{27}$) |
| 23 | 1646 | 1580 | 16 | υ [R1 (C-C-C)] + β ($C_{17}$-$H_{29}$, $C_{18}$-$H_{30}$) |
| 24 | 1768 | 1697 | 789 | υ ($C_{12}$-$O_2$, $C_{13}$-$O_3$) |
| 25 | 1778 | 1707 | 532 | υ ($C_{10}$-$O_1$, $C_{14}$-$O_4$) + β ($N_6$-$H_{28}$) |
| 26 | 1790 | 1718 | 160 | υ ($C_{10}$-$O_1$, $C_{14}$-$O_4$) |
| 27 | 1823 | 1750 | 76 | υ ($C_{12}$-$O_2$, $C_{13}$-$O_3$) |
| 28 | 3055 | 2932 | 17 | υ ($C_{11}$-$H_{25,26,27}$) |
| 29 | 3059 | 2936 | 16 | υ ($C_8$-$H_{21}$, $C_8$-$H_{22}$) |
| 30 | 3560 | 3417 | 53 | υ ($N_6$-$H_{28}$) |

Abbreviations: υ – stretching, $\upsilon_{as}$ – antisymmetric stretching, β – in plane bending, γ – out of plane, bending, χ – scissoring, ρ – shrinking, τ – twisting, ω – wagging, R – rocking.

In lower frequency regions, some C–H bending mode of vibration along with mixing of other mode of vibration appears in both molecules. The C–H in-plane bending mode appears at 1084 $cm^{-1}$, 978 $cm^{-1}$ in molecule A, while corresponding mode appears at 1178 $cm^{-1}$, 1162 $cm^{-1}$ in its molecule B along with mixing of several other bonds. The C–H out of plane bending mode appears at 702 $cm^{-1}$ in molecule A, while corresponding mode appears at 701 $cm^{-1}$ in its molecule B along with mixing of several other bonds.

**Methylene (=$CH_2$) and methyl (–$CH_3$) group vibrations**

The methylene (=$CH_2$) and methyl (–$CH_3$) group due to internal coordinate arrangement [21], having six different modes of vibration namely asymmetric, symmetric stretch, rocking, scissoring, twisting as well as wagging. In general, symmetric stretching –$CH_2$/$CH_3$ appears lower frequencies region due to weaker bond strength and characteristic region for symmetric –CH2/CH3 observed in between 2900 $cm^{-1}$ – 3000 $cm^{-1}$ however antisymmetric stretching vibration for –CH2/CH3 observed some higher frequencies region 3100 $cm^{-1}$ – 3000 $cm^{-1}$ due to strong bond strength [1]. In present study, twisting in methylene (=CH2) group appears at 1225 $cm^{-1}$, 1158 $cm^{-1}$, 1150 $cm^{-1}$, 1084 $cm^{-1}$ in molecule A, while in its molecule B, the corresponding peak appears respectively at 1288 $cm^{-1}$, 1255 $cm^{-1}$, 1199 $cm^{-1}$, 1162 $cm^{-1}$ along with mixing of several other bonds. In molecule A,

wagging in methylene (=CH2) group appears at 1307 $cm^{-1}$, 1268 $cm^{-1}$, 1158 $cm^{-1}$, while corresponding peak in its molecule B appears at 1336 $cm^{-1}$, 1329 $cm^{-1}$, 1255 $cm^{-1}$ respectively along with mixing of several other bonds.

In the methyl (–CH3) group, significant lower frequency peak due to rocking appears at 742 $cm^{-1}$, 548 $cm^{-1}$ in its molecule A. In molecule B, the wagging in methyl ($–CH_3$) group appears at 862 $cm^{-1}$ in its molecule B along with mixing of several other bonds.

**C–C vibrations**

The stretching frequency of a carbon-carbon (C–C) bond in infrared (IR) spectroscopy varies depending on the bond type (single, double, or triple). Generally, C–C single bonds appear in the region of 1200–800 $cm^{-1}$, C=C double bonds around 1680–1640 $cm^{-1}$, and C≡C triple bonds at significantly higher frequencies, typically 2300–2050 $cm^{-1}$ [37]. In present study, the significant intense peak due to C–C–C stretching mode in R1 appears at 1342 $cm^{-1}$, 1324 $cm^{-1}$ in molecule A, while the corresponding peak in its molecule B appears at 1336 $cm^{-1}$, 1297 $cm^{-1}$ respectively. In lower frequency regions, the C–C in-plane bending mode in molecule A appears at 864 $cm^{-1}$, while the corresponding peak in its molecule B appears at 862 $cm^{-1}$.

**–C=O absorption vibration**

The absorption band of the carbonyl group (C=O) sharp stretching modes of vibration is observed in between 1670–1820 $cm^{-1}$ [8]. In present study, the very high intense –C=O absorption peaks due to stretching of both carbon and oxygen appears at 1711 $cm^{-1}$, 1702 $cm^{-1}$ in molecule A, while the corresponding high intense peaks in its molecule B appears at 1707 $cm^{-1}$, 1697 $cm^{-1}$ respectively. The intense –C=O absorption peaks also appear at 1754 $cm^{-1}$, 1723 $cm^{-1}$ in molecule A, while corresponding peaks appears respectively at 1750 $cm^{-1}$, 1718 $cm^{-1}$ in its molecule B. The variation in –C=O absorption peaks in both molecules is 5 $cm^{-1}$. In molecule A, the –C=O out of plane bending mode appears at 702 $cm^{-1}$, while in its molecule B, it appears at 742 $cm^{-1}$. In molecule A, the –C=O in-plane bending mode appears at 588 $cm^{-1}$, while the corresponding peak appears at 584 $cm^{-1}$ in its molecule B.

**C–N vibrational mode**

The C–N single bond stretching vibration typically appears in the fingerprint region 1200–700 $cm^{-1}$ of an infrared (IR) spectrum. In present study, the very high intense peaks due to C–N stretching mode in molecule A appears at 1342 $cm^{-1}$, 1158

$cm^{-1}$, while the corresponding peaks in its molecule B appears at 1297 $cm^{-1}$, 1162 $cm^{-1}$ respectively. In molecule A, rest of the C–N stretching mode appears at 1324 $cm^{-1}$, 1268 $cm^{-1}$, 1084 $cm^{-1}$, while the corresponding peaks appears at 1288 $cm^{-1}$, 1178 $cm^{-1}$, 1027 $cm^{-1}$ in its molecule B, respectively.

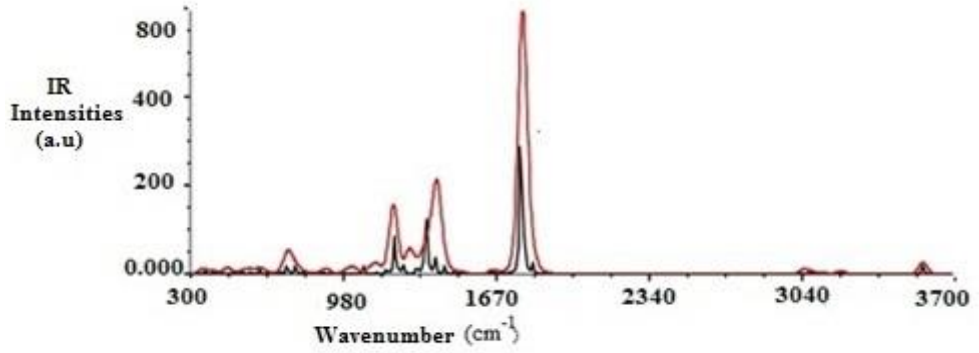


Fig. 3. Compare computed IR spectra of molecule A (red), and molecule B (black).

## NBO ANALYSIS

The Natural bonding orbitals (NBO) analysis is most significant technique to explore charge transfers or conjugative interactions in various systems. The interaction strength is directly related with second order lowering energy $E^{(2)}$. The lowering energy $E^{(2)}$ is calculated for each acceptor NBO($j$) and, donor NBO($i$) [17, 39].

$$E^{(2)} = -q_i \frac{F_{ij}^2}{E_i - E_j} \tag{13}$$

Where $q_i$ is donor orbital occupancy; $E_i$, $E_j$ are energies of acceptor and donor NBO orbitals respectively. The donor molecular orbital and its occupancies, acceptor molecular orbitals and their occupancies $F_{ij}$ is the off-diagonal Fock matrices. In the molecule A and the molecule B, a significant contribution appears transition in between donor to acceptor orbitals in between Lp→σ*, Lp→π*. The electron density of donor orbital varies from 1.63088e to 1.87215e in molecule A however corresponding electron density varies from 1.63547e to 1.85561e in its molecule B. A significant contribution arises due to electron transition from $Lp(2)O_1 \rightarrow \sigma^*(N_6\text{-}C_{10})$ which stabilizes the system molecule A by 25.65 kcal/mol and its molecule B by 26.83 kcal/mol. In $Lp(2)O_2 \rightarrow \sigma^*(N_5\text{-}C_{11})$ electron transition, the system is stabilized by 28.22 kcal/mol in the molecule A and in the molecule B by 28.93

kcal/mol in the corresponding transition respectively. In $Lp(2)O_3 \rightarrow \sigma^*(N_5\text{-}C_{12})$ electron transition, the system of the molecule A is stabilized by 28.21 kcal/mol while in corresponding electron transition in the molecule B the system gets stabilized by 30.03 kcal/mol. Another transition appears due to electron transition in $Lp(2)O_4 \rightarrow \sigma^*(N_6\text{-}C_{15})$, the system gets stabilized by 26.05 kcal/mol in the molecule A and 27.46 kcal/mol in the molecule B. The important charge transfer appears in $Lp(1)N_5 \rightarrow \pi^*(O_2\text{-}C_{11})$ and $Lp(1)N_5 \rightarrow \pi^*(O_3\text{-}C_{12})$, the system of the molecule A gets stabilized by 52.54 kcal/mol and 52.87 kcal/mol respectively while in corresponding transitions, the system of its molecule B gets stabilized by 47.22 kcal/mol and 47.66 kcal/mol respectively. The charge transfer in between $Lp(1)N_6 \rightarrow \pi^*(O_4\text{-}C_{15})$ stabilize up to 49.63 kcal/mol and 47.69 kcal/mol of molecules A and B respectively which is further enhance in $Lp(1)N_6 \rightarrow \pi^*(O_1\text{-}C_{10})$ stabilized up to 50.60 kcal/mol and 51.02 kcal/mol in molecules A and B respectively.

In the electron transition of $\sigma \rightarrow \sigma^*$, the electron density of donor orbital varies from 1.95635e to 1.98156e in molecule A however in the molecule B, the electron density of donor orbital varies from 1.96232e to 1.98073e, but in this charge transfer the system gets stabilized by low energy near to 4–5 kcal/mol.

In the charge transfer of $\pi(C_{13}\text{-}C_{16}) \rightarrow \pi^*(O_2\text{-}C_{11})$, the system of molecule A gets stabilized by 19.85 kcal/mol while in corresponding transition of its molecule B, the system gets stabilized by 17.78 kcal/mol. In $\pi(C_{13}\text{-}C_{16}) \rightarrow \pi^*(C_{14}\text{-}C_{17})$ electron transition, the system of molecule A gets stabilized by 20.91 kcal/mol while in corresponding transition of its molecule B, the system gets stabilized by 21.33 kcal/mol. In the charge transfer of $\pi(C_{18}\text{-}C_{19}) \rightarrow \pi^*(C_{13}\text{-}C_{16})$ and $\pi(C_{18}\text{-}C_{19}) \rightarrow \pi^*(C_{14}\text{-}C_{17})$ in the molecule A, the system gets stabilized by 19.84 kcal/mol and 19.42 kcal/mol respectively, however in the corresponding charge transfer in its molecule B, the system gets stabilized by 19.83 kcal/mol and 19.34 kcal/mol respectively.

*Table 6*

NBO analysis of molecule A by using combination of of DFT/B3LYP method and 6-311+G(d,p) basis set

| **Donor NBO (*i*)** | **Occupancy (*i*)** (a.u) | **Acceptor NBO (*j*)** | **Occupancy (*j*)** (a.u) | $E^{(2)}$ (kcal/mol) | $E_j - E_i$ (a.u) | $F(i,j)$ (a.u) |
|---|---|---|---|---|---|---|
| $\pi(O_2\text{-}C_{11})$ | 1.96935 | $\pi^*(C_{13}\text{-}C_{16})$ | 0.34031 | 4.54 | 0.42 | 0.042 |
| $\pi(O_3\text{-}C_{12})$ | 1.96931 | $\pi^*(C_{14}\text{-}C_{17})$ | 0.34044 | 4.40 | 0.42 | 0.042 |
| $\sigma(C_7\text{-}H_{20})$ | 1.95635 | $\pi^*(O_1\text{-}C_{10})$ | 0.22321 | 6.36 | 0.53 | 0.054 |

| | | | | | | |
|---|---|---|---|---|---|---|
| $\sigma(C_7\text{-}H_{20})$ | 1.95635 | $\sigma^*(N_5\text{-}C_{12})$ | 0.08840 | 4.34 | 0.95 | 0.058 |
| $\sigma(C_9\text{-}H_{23})$ | 1.96137 | $\pi^*(O_4\text{-}C_{15})$ | 0.21745 | 6.57 | 0.52 | 0.055 |
| $\sigma(C_{11}\text{-}C_{13})$ | 1.96802 | $\sigma^*(N_5\text{-}C_7)$ | 0.03746 | 4.96 | 1.01 | 0.063 |
| $\sigma(C_{11}\text{-}C_{13})$ | 1.96802 | $\sigma^*(C_{14}\text{-}C_{17})$ | 0.02319 | 4.31 | 1.24 | 0.065 |
| $\sigma(C_{12}\text{-}C_{14})$ | 1.96925 | $\sigma^*(N_5\text{-}C_7)$ | 0.03746 | 4.77 | 1.01 | 0.062 |
| $\sigma(C_{12}\text{-}C_{14})$ | 1.96925 | $\sigma^*(C_{13}\text{-}C_{16})$ | 0.02245 | 4.27 | 1.26 | 0.066 |
| $\sigma(C_{13}\text{-}C_{14})$ | 1.96238 | $\sigma^*(C_{13}\text{-}C_{16})$ | 0.02245 | 4.96 | 1.29 | 0.072 |
| $\sigma(C_{13}\text{-}C_{14})$ | 1.96238 | $\sigma^*(C_{14}\text{-}C_{17})$ | 0.02319 | 4.77 | 1.27 | 0.070 |
| $\sigma(C_{13}\text{-}C_{16})$ | 1.97554 | $\sigma^*(C_{13}\text{-}C_{14})$ | 0.02928 | 5.43 | 1.30 | 0.075 |
| $\pi(C_{13}\text{-}C_{16})$ | 1.63035 | $\pi^*(O_2\text{-}C_{11})$ | 0.24824 | 19.85 | 0.27 | 0.067 |
| $\pi(C_{13}\text{-}C_{16})$ | 1.63035 | $\pi^*(C_{14}\text{-}C_{17})$ | 0.34044 | 20.91 | 0.30 | 0.071 |
| $\sigma(C_{14}\text{-}C_{17})$ | 1.97442 | $\sigma^*(C_{13}\text{-}C_{14})$ | 0.02928 | 5.43 | 1.30 | 0.075 |
| $\pi(C_{14}\text{-}C_{17})$ | 1.62911 | $\pi^*(O_3\text{-}C_{12})$ | 0.24852 | 20.04 | 0.27 | 0.067 |
| $\pi(C_{14}\text{-}C_{17})$ | 1.62911 | $\pi^*(C_{13}\text{-}C_{16})$ | 0.34031 | 21.29 | 0.29 | 0.071 |
| $\sigma(C_{16}\text{-}C_{18})$ | 1.97902 | $\sigma^*(C_{11}\text{-}C_{13})$ | 0.06598 | 4.61 | 1.16 | 0.066 |
| $\sigma(C_{16}\text{-}H_{26})$ | 1.97927 | $\sigma^*(C_{13}\text{-}C_{14})$ | 0.02928 | 4.37 | 1.11 | 0.062 |
| $\sigma(C_{17}\text{-}C_{19})$ | 1.97719 | $\sigma^*(C_{12}\text{-}C_{14})$ | 0.06626 | 4.81 | 1.16 | 0.067 |
| $\sigma(C_{17}\text{-}C_{19})$ | 1.97719 | $\sigma^*(C_{14}\text{-}C_{17})$ | 0.02319 | 5.19 | 1.27 | 0.073 |
| $\sigma(C_{17}\text{-}C_{19})$ | 1.97719 | $\pi^*(C_{18}\text{-}C_{19})$ | 0.31494 | 29.77 | 4.18 | 0.341 |
| $\sigma(C_{17}\text{-}H_{27})$ | 1.97914 | $\sigma^*(C_{13}\text{-}C_{14})$ | 0.02928 | 4.31 | 1.11 | 0.062 |
| $\sigma(C_{18}\text{-}C_{19})$ | 1.98108 | $\sigma^*(C_{17}\text{-}H_{27})$ | 0.01462 | 4.92 | 1.14 | 0.067 |
| $\sigma(C_{18}\text{-}C_{19})$ | 1.98108 | $\pi^*(C_{18}\text{-}C_{19})$ | 0.31494 | 12.37 | 4.18 | 0.220 |
| $\sigma(C_{18}\text{-}C_{19})$ | 1.98108 | $\sigma^*(C_{18}\text{-}H_{28})$ | 0.01245 | 22.28 | 4.18 | 0.273 |
| $\pi(C_{18}\text{-}C_{19})$ | 1.63395 | $\pi^*(C_{13}\text{-}C_{16})$ | 0.34031 | 19.84 | 0.29 | 0.068 |
| $\pi(C_{18}\text{-}C_{19})$ | 1.63395 | $\pi^*(C_{14}\text{-}C_{17})$ | 0.34044 | 19.42 | 0.29 | 0.068 |
| $\sigma(C_{19}\text{-}H_{29})$ | 1.98156 | $\sigma^*(C_{14}\text{-}C_{17})$ | 0.02319 | 4.93 | 1.08 | 0.065 |
| $\sigma(C_{19}\text{-}H_{29})$ | 1.98156 | $\pi^*(C_{18}\text{-}C_{19})$ | 0.31494 | 49.95 | 3.99 | 0.432 |
| $\sigma(C_{19}\text{-}H_{29})$ | 1.98156 | $\sigma^*(C_{18}\text{-}H_{28})$ | 0.01245 | 46.61 | 3.99 | 0.386 |

| | | | | | | |
|---|---|---|---|---|---|---|
| $Lp(2)O_1$ | 1.86501 | $\sigma^*(N_6\text{-}C_{10})$ | 0.07943 | 25.65 | 0.67 | 0.119 |
| $Lp(2)O_1$ | 1.86501 | $\sigma^*(C_7\text{-}C_{10})$ | 0.07605 | 18.78 | 0.63 | 0.098 |
| $Lp(2)O_2$ | 1.86096 | $\sigma^*(N_5\text{-}C_{11})$ | 0.08932 | 28.22 | 0.69 | 0.126 |
| $Lp(2)O_2$ | 1.86096 | $\sigma^*(C_{11}\text{-}C_{13})$ | 0.06598 | 17.36 | 0.73 | 0.102 |
| $Lp(2)O_3$ | 1.86275 | $\sigma^*(N_5\text{-}C_{12})$ | 0.08840 | 28.21 | 0.69 | 0.126 |
| $Lp(2)O_3$ | 1.86275 | $\sigma^*(C_{12}\text{-}C_{14})$ | 0.06626 | 17.42 | 0.73 | 0.102 |
| $Lp(2)O_4$ | 1.87215 | $\sigma^*(N_6\text{-}C_{15})$ | 0.08226 | 26.05 | 0.67 | 0.120 |
| $Lp(2)O_4$ | 1.87215 | $\sigma^*(C_9\text{-}C_{15})$ | 0.05622 | 16.81 | 0.64 | 0.095 |
| $Lp(1)N_5$ | 1.63202 | $\pi^*(O_2\text{-}C_{11})$ | 0.24824 | 52.54 | 0.29 | 0.113 |
| $Lp(1)N_5$ | 1.63202 | $\pi^*(O_3\text{-}C_{12})$ | 0.24852 | 52.87 | 0.28 | 0.113 |
| $Lp(1)N_5$ | 1.63202 | $\sigma^*(C_7\text{-}C_8)$ | 0.02265 | 4.29 | 0.65 | 0.052 |
| $Lp(1)N_5$ | 1.63202 | $\sigma^*(C_7\text{-}C_{10})$ | 0.07605 | 5.38 | 0.64 | 0.057 |
| $Lp(1)N_6$ | 1.63088 | $\pi^*(O_1\text{-}C_{10})$ | 0.22321 | 50.60 | 0.28 | 0.110 |
| $Lp(1)N_6$ | 1.63088 | $\pi^*(O_4\text{-}C_{15})$ | 0.21745 | 49.63 | 0.28 | 0.110 |
| $\pi^*(O_2\text{-}C_{11})$ | 0.24824 | $\pi^*(C_{13}\text{-}C_{16})$ | 0.34031 | 95.37 | 0.02 | 0.079 |
| $\pi^*(O_3\text{-}C_{12})$ | 0.24852 | $\pi^*(C_{14}\text{-}C_{17})$ | 0.34044 | 72.84 | 0.03 | 0.079 |

*Table 7*

NBO analysis of Molecule B by using combination of DFT/B3LYP method and 6-311+G(d,p) basis set

| **Donor NBO (*i*)** | **Occupancy (*i*)** | **Acceptor NBO (*j*)** | **Occupancy (*j*)** | $E^{(2)}$ (kcal/mol) | $E_j–E_i$ (a.u.) | $F(i,j)$ (a.u.) |
|---|---|---|---|---|---|---|
| $\sigma(C_7\text{-}C_{11})$ | 1.96232 | $\sigma^*(O_1\text{-}C_{10})$ | 0.01029 | 4.25 | 0.63 | 0.049 |
| $\sigma(C_{12}\text{-}C_{15})$ | 1.97155 | $\sigma^*(C_{16}\text{-}C_{18})$ | 0.02168 | 4.14 | 1.25 | 0.064 |
| $\sigma(C_{13}\text{-}C_{16})$ | 1.97075 | $\sigma^*(C_{15}\text{-}C_{17})$ | 0.02279 | 4.12 | 1.22 | 0.063 |
| $\sigma(C_{15}\text{-}H_{16})$ | 1.96400 | $\sigma^*(C_{15}\text{-}H_{17})$ | 0.02279 | 4.53 | 1.26 | 0.068 |
| $\sigma(C_{15}\text{-}H_{16})$ | 1.96400 | $\sigma^*(C_{16}\text{-}C_{18})$ | 0.02168 | 4.58 | 1.28 | 0.069 |
| $\sigma(C_{15}\text{-}C_{17})$ | 1.97478 | $\sigma^*(C_{15}\text{-}H_{16})$ | 0.02735 | 5.30 | 1.30 | 0.074 |

| | | | | | | |
|---|---|---|---|---|---|---|
| $\sigma(C_{15}-C_{17})$ | 1.97478 | $\pi^*(O_2-C_{12})$ | 0.23950 | 18.62 | 0.27 | 0.066 |
| $\sigma(C_{15}-C_{17})$ | 1.97478 | $\pi^*(C_{16}-C_{18})$ | 0.33699 | 20.44 | 0.29 | 0.070 |
| $\sigma(C_{16}-C_{18})$ | 1.97596 | $\sigma^*(C_{15}-C_{16})$ | 0.06953 | 5.12 | 1.30 | 0.073 |
| $\pi(C_{16}-C_{18})$ | 1.63494 | $\pi^*(O_3-C_{13})$ | 0.23843 | 17.78 | 0.27 | 0.064 |
| $\pi(C_{16}-C_{18})$ | 1.63494 | $\pi^*(C_{15}-C_{17})$ | 0.33932 | 21.33 | 0.29 | 0.071 |
| $\pi(C_{16}-C_{18})$ | 1.63494 | $\pi^*(C_{19}-C_{20})$ | 0.31064 | 15.34 | 0.35 | 0.066 |
| $\sigma(C_{17}-C_{19})$ | 1.97690 | $\sigma^*(C_{12}-C_{15})$ | 0.06915 | 4.82 | 1.13 | 0.067 |
| $\sigma(C_{17}-H_{29})$ | 1.97938 | $\sigma^*(C_{15}-C_{16})$ | 0.02735 | 1.33 | 1.10 | 0.062 |
| $\sigma(C_{18}-C_{20})$ | 1.97857 | $\sigma^*(C_{13}-C_{16})$ | 0.06953 | 4.64 | 1.13 | 0.065 |
| $\sigma(C_{18}-H_{30})$ | 1.97857 | $\sigma^*(C_{15}-C_{16})$ | 0.02735 | 4.34 | 1.10 | 0.062 |
| $\sigma(C_{19}-C_{20})$ | 1.98073 | $\sigma^*(C_{19}-H_{31})$ | 0.01288 | 12.77 | 3.45 | 0.188 |
| $\pi(C_{19}-C_{20})$ | 1.63924 | $\pi^*(C_{15}-C_{17})$ | 0.33932 | 19.83 | 0.29 | 0.068 |
| $\pi(C_{19}-C_{20})$ | 1.63924 | $\pi^*(C_{16}-C_{18})$ | 0.33699 | 19.34 | 0.29 | 0.067 |
| $Lp(2)O_1$ | 1.85561 | $\sigma^*(N_6-C_{10})$ | 0.08085 | 26.83 | 0.68 | 0.123 |
| $Lp(2)O_1$ | 1.85561 | $\sigma^*(C_7-C_{10})$ | 0.08683 | 21.12 | 0.60 | 0.102 |
| $L(2)O_2$ | 1.84977 | $\sigma^*(N_5-C_{12})$ | 0.09113 | 28.93 | 0.65 | 0.125 |
| $Lp(2)O_2$ | 1.84977 | $\sigma^*(C_{12}-C_{15})$ | 0.06915 | 19.30 | 0.70 | 0.106 |
| $Lp(2)O_3$ | 1.85392 | $\sigma^*(N_5-C_{13})$ | 0.09454 | 30.03 | 0.65 | 0.126 |
| $Lp2)O_3$ | 1.85392 | $\sigma^*(C_{13}-C_{16})$ | 0.06953 | 18.86 | 0.69 | 0.104 |
| $Lp(2)O_4$ | 1.86469 | $\sigma^*(N_6-C_{14})$ | 0.08558 | 27.46 | 0.67 | 0.123 |
| $Lp(2)O_4$ | 1.86469 | $\sigma^*(C_9-C_{14})$ | 0.05970 | 18.82 | 0.64 | 0.100 |
| $Lp(1)N_5$ | 1.63757 | $\pi^*(O_2-C_{12})$ | 0.23950 | 47.22 | 0.28 | 0.105 |
| $Lp(1)N_5$ | 1.63757 | $\pi^*(O_3-C_{13})$ | 0.23843 | 47.66 | 0.28 | 0.106 |
| $Lp(1)N_6$ | 1.63547 | $\pi^*(O_1-C_{10})$ | 0.22274 | 51.02 | 0.29 | 0.112 |
| $Lp(1)N_6$ | 1.63547 | $\pi^*(O_4-C_{14})$ | 0.21412 | 47.69 | 0.29 | 0.109 |
| $\pi(O_2-C_{12})$ | 1.97269 | $\pi^*(C_{15}-C_{17})$ | 0.33932 | 132.30 | 0.02 | 0.077 |
| $\pi(O_3-C_{13})$ | 1.97326 | $\pi^*(C_{16}-C_{18})$ | 0.33699 | 96.08 | 0.02 | 0.075 |
| $\pi(C_{15}-C_{17})$ | 1.63317 | $\pi^*(C_{19}-C_{20})$ | 0.31064 | 45.13 | 0.06 | 0.081 |

| | | | | | | |
|---|---|---|---|---|---|---|
| $\pi(C_{16}\text{-}C_{18})$ | 1.63494 | $\pi^*(C_{19}\text{-}C_{20})$ | 0.31064 | 77.06 | 0.05 | 0.101 |

## BIOLOGICAL PROPERTIES AND BIOLOGICAL ACTIVITIES

ALOGPS 2.1 program built on electro topological indices *e.g.* log *P* and log *S* [41, 48]. The value of log *P*, log *S* and other parameters like number of atoms molecular weight, molar refractivity (*MR*) for both molecules A and B are computed and listed in Table 8. This computed log *P* for both molecules A and B is greater than 5 means both molecules simply transport through cell membranes to show their good pharmacological behavior. The predicted log *S* in between −1 to −6 for both molecules A and B falls within range corresponding value of 85 % drugs. The computed log *S* for both molecules A and B shows that both molecules A and B indicate good permeability through membranes.

The tentatively intended drug likeliness is predicted by molar refractivity (*MR*) which established its orally active drugs for humans. The value of *MR* for oral drug falls within range 40 and 130. The molar refractive *MR* of any drug is calculated by below equation [11, 26].

$$MR = \left[\frac{n^2-1}{n^2+2}\right]\left(\frac{MW}{\rho}\right) = 1.33\alpha\pi N \tag{14}$$

In this equation N stands for Avogadro number, and α stands for mean polarizability. Lipinski's five-rule could utilize to identification of the compound by drug-likeness [6, 20]. According to five rules for drug-likeness both title compound falls in category of good drug because number of atoms in molecules A and B lies in between 20−70 atoms, molecular weight of molecule A and B lies within range 180–500 computed ionophilicity of both molecules A and B log *P* > 5. The computed molar refractive *MR* for both molecules A and B lies in between 40−130 to become good oral drug, some biological activities of both molecules A and B are computed by PASS online server [35] listed in Table 9 for Pa > 70 %. The using PASS on line server predict several biological activities *e.g.* mutagenicity, carcinogenicity, teratogenicity and embryo toxicity etc of biological active molecules. The molecule A shows activity against CYP2C12 substrate (0.973), Nicotinic alpha2beta2 receptor antagonist (0.861), CYP2A8 substrate (0.754), Testosterone 17beta-dehydrogenase ($NADP^+$) inhibitor (0.727), CYP2C11 substrate (0.685) etc however molecule B shows biological activity against CYP2C12 substrate (0.906), antiarthritic (0.854), tumor necrosis factor alpha release inhibitor (0.813), testosterone 17beta-dehydrogenase ($NADP^+$) inhibitor (9.744), etc. The molecule A shown more activity against CYP2C12 substrate than molecule B however molecule B shows more activity against testosterone 17beta-dehydrogenase ($NADP^+$) inhibitor as compared

to molecule A. The rat cytochrome P450 enzyme is known as CYP2C12 which metabolizes numerous substrates, with 7-hydroxy-3-(4-methoxyphenyl)-4-methyl coumarin and arachidonic acid metabolites. Growth hormone (GH) can stimulate the appearance of CYP2C12, and the enzyme's activity is complicated in growth hormone signaling trails, potentially over the creation of eicosanoids [33]. Testosterone 17-beta-dehydrogenase ($NADP^+$) inhibitor are utilized in treating hormone-dependent diseases *e.g.*, certain cancers, acne, and endometriosis by controlling the production of active steroid hormones [44].

## MOLECULAR DOCKING

The computational technique which utilized in drug discovery is termed as molecular docking. The molecular docking is designed to forecast the mode of binding in terms of affinity of ligand with a target protein. In docking procedures, one can evaluate binding affinity in between ligand-receptor complex on basis of Newtonian mechanics. The energy connected with each believable configuration of the ligand are computed. The full fitness score (FS) binding affinity bond length are used to strengthen and then used to compute strength of binding between ligand with a target protein. The Swiss Dock [43] is online server used to predict target protein and binding with molecules A and B. The docking process is blind creased to avoid sampling bias by pervasive the whole receptor molecule not assigning any specific part of the protein. Swiss dock predicts P2X7 protein receptor (PDB ID: P2X7) for docking with both molecules A and B.

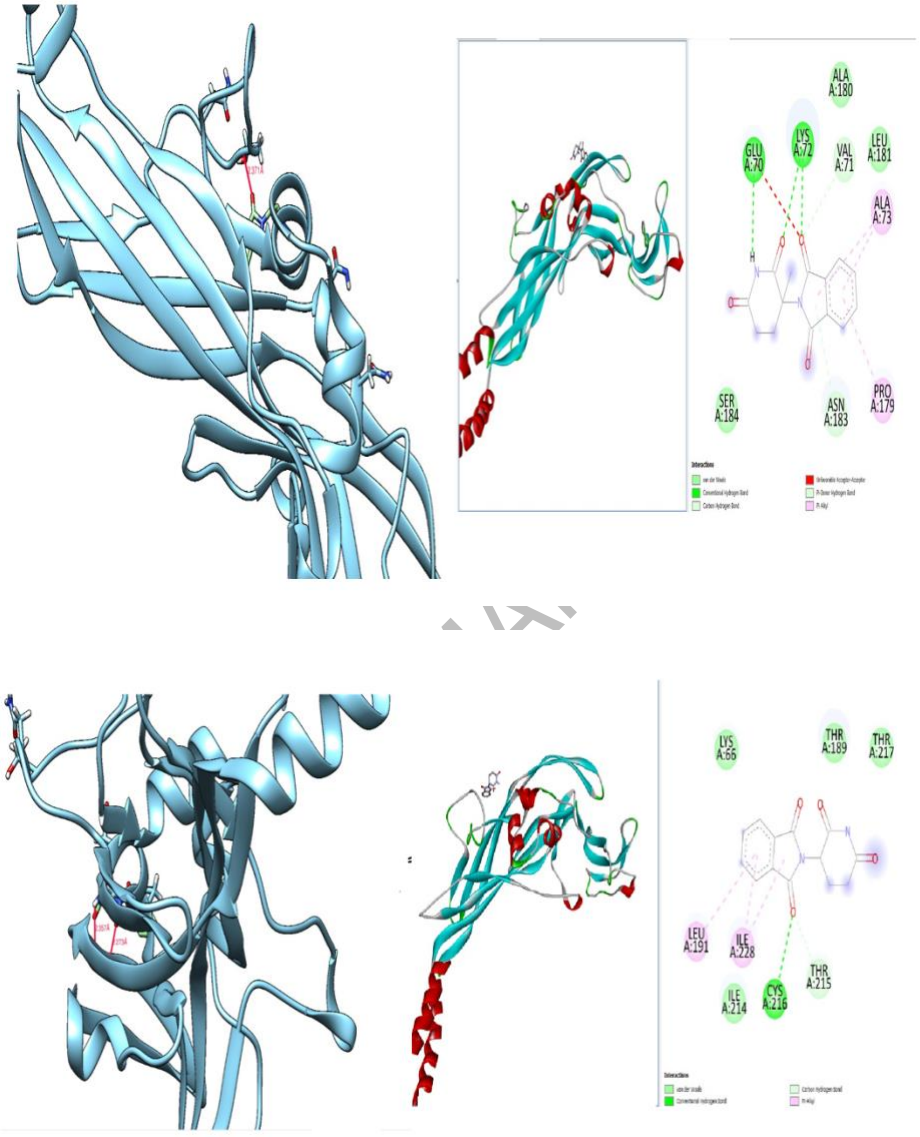


Fig. 4. Molecular docking picture of molecule A (upper), and molecule B (lower) with P2X7 protein.

*Table 8*

Various transport and docking properties of molecules A and B

| Mole. | log *P* | log *S* | H-BOND (Å) | Atoms | Residue | Δ*G* (kcal/mol) | *MR* | Molecular weight | Atoms |
|---|---|---|---|---|---|---|---|---|---|
| A | 5.42 | –3.00 | 2.35<br>2.27 | O1 | VALA:71<br>ASNA: 183 | –5.60 | 134.18 | 101.79 | 32 |
| B | 5.92 | –3.45 | 2.37 | O2 | ALU70 | –5.70 | 124.91 | 96.51 | 29 |

*Table 9*

Computed activities of molecules A and B by using PASS online server

| S.N. | Activities | *P*i | *P*a | Activities | *P*i | *P*a |
|---|---|---|---|---|---|---|
| | Molecule A | | | Molecule B | | |
| 1 | CYP2C12 substrate | 0.973 | 0.002 | CYP2C12 substrate | 0.906 | 0.011 |
| 2 | Nicotinic alpha2beta2 receptor antagonist | 0.861 | 0.005 | Antiarthritic | 0.854 | 0.005 |
| 3 | Nicotinic alpha6beta3beta4alpha5 receptor antagonist | 0.827 | 0.007 | Tumour necrosis factor alpha release inhibitor | 0.813 | 0.004 |
| 4 | CYP2A8 substrate | 0.754 | 0.005 | Inflammatory Bowel disease treatment | 0.787 | 0.004 |
| 5 | Nootropic | 0.755 | 0.026 | Anticonvulsant | 0.756 | 0.007 |
| 6 | Mannan endo-1,4-beta-mannosidase inhibitor | 0.725 | 0.004 | Mannan endo-1,4-beta-mannosidase inhibitor | 0.729 | 0.004 |
| 7 | Pterin deaminase inhibitor | 0.710 | 0.011 | $H^+$-transporting two-sector ATPase inhibitor | 0.720 | 0.005 |
| 8 | Interleukin 2 agonist | 0.698 | 0.003 | Testosterone 17beta-dehydrogenase (NADP+) inhibitor | 0.744 | 0.041 |
| 9 | Testosterone 17beta-dehydrogenase (NADP+) inhibitor | 0.727 | 0.046 | Pterin deaminase inhibitor | 0.707 | 0.011 |
| 10 | CYP2C11 substrate | 0.685 | 0.008 | Transplant rejection treatment | 0.700 | 0.004 |
| 11 | Tumour necrosis factor alpha release inhibitor | 0.652 | 0.005 | Lysase inhibitor | 0.640 | 0.034 |

The P2X7 is protein is extracellular ATP-gated ion channel which plays important role in immune responses, *e.g.*, inflammation, as well as complicated in

other cellular developments like cell explosion and death. The function of P2X7 protein is different depended on ATP concentration. Small ATP concentration unlocks a channel for small cations ($Ca^{2+}$, $Na^{+}$, $K^{+}$) however higher ATP concentration leads cell death [46]. For docking of P2X7 receptor protein with molecules A and B upload its mole 2 files and pdb file of P2X7R. The docking picture of P2X7R with molecule As A and B are shown in Figure 4.

The O1, O2 molecule A shown two hydrogen bond receptors VALA:71, ASNA: 183 with binding affinity −5.60 kcal/mol however O1 atom molecule B interact with ALU70 receptor of targeted protein with bond length 2.37 with lower binding affinity −5.70 kcal/mol. The computed binding affinity and full fitness score shows that both molecule A and B bind well with targeted protein,

## CONCLUSION

The geometry of both molecules A and B optimized by using DFT/B3LYP method. The substitution of $-CH_3$ group in molecule B make angular distortion of on glutarimide ring. The substitution of methyl group ($-CH_3$) withdrawn charge from glutarimide ring originate more polarity in molecule B which is also reflects by computed HOMO and LUMO gap molecule A and molecule B. The Fukai function analysis shows that $O_4$ is the most reactive site for nucleophilic attack in the molecule A and $C_{12}$ is most reactive site in its molecule B for the nucleophilic attack. The NBO analysis shows that most significant contribution appears due to charge transfer in between $Lp(1)N_6 \rightarrow \pi^*(O_1\text{-}C_{10})$ which stabilized up to 50.60 kcal/mol and 51.02 kcal/mol in molecules A and B respectively. Both molecules A and B qualify Lipinski's five rule for drug-likeness so both molecule falls in category of good oral drug. The using PASS online server predict biological activity against CYP2C12 substrate (0.973) and substrate (0.906) for molecules A and B respectively. The docking of both molecules A and B has been performed by P2X7R protein. The two-hydrogen bond appears in between atoms $O_1$, $O_2$ of the molecule A with receptor VALA: 71, ASNA: 183 of targeted protein with binding affinity −5.60 kcal/mol. On other hand one hydrogen bond appears in between $O_1$ atom of the molecule B with ALU70 receptor of targeted protein with lower binding affinity −5.70 kcal/mol. The computed binding affinity and full fitness score show that both molecules A and B bind well with targeted protein. All calculation has been performed on single molecule in gas phase, so we have ignored molecular interactions and solvent effect.

## REFERENCES


1. ABRAHAM, C.S., S. MUTHU, J.C. PRASANA, S. ARMAKOVIĆ, S.J. ARMAKOVIĆ, B. GEOFFREY, Computational evaluation of the reactivity and pharmaceutical potential of an organic amine: a DFT, molecular dynamics simulations and molecular docking approach, *Spectrochim. Acta A Mol. Biomol. Spectrosc*., 2019, **222**, 117188, https://doi.org/10.1016/j.saa.2019.117188.
2. ANDERSSON, M.P., P. UVDAL, New scale factors for harmonic vibrational frequencies using the B3LYP density functional method with the triple-ζ basis set 6-311+G(d,p), *J. Phys. Chem. A*, 2005, **109**(12), 2937–2941, https://doi.org/10.1021/jp045733a.
3. BECKE, A.D., Density-functional thermochemistry, III. The role of exact exchange, *J. Chem. Phys.,* 1993, **98**, 5648–5652, https://doi.org/10.1063/1.464913.
4. BLAKEMORE, C., S. JENNETT, *The Oxford Companion to the Body*., Oxford University Press, 2003, pp. 682–684, https://doi.org/10.1093/acref/9780198524038.001.0001.
5. CHATTARAJ, P.K., U. SARKAR, D.R. ROY, Electrophilicity index, *Chem. Rev.,* 2006, **106**, 2065–2091, https://doi.org/10.1021/cr040109f.
6. CHOW, H., H. CHEN, T. NG, P. MYRDAL, S.H. YALKOWSKY, Using backpropagation networks for the estimation of aqueous activity coefficients of aromatic organic compounds, *J. Chem. Inf. Comput. Sci.,* 1995, **35**(4), 723–728, https://doi.org/10.1021/ci00026a009.
7. COLTHUP, N.B., L.H. DALY, S.E. WIBERLEY, *Introduction to Infrared and Raman Spectroscopy*, Academic Press, New York, 1990, ISBN: https://doi.org/10.1016/C2009-0-21628-X.
8. ERDOGDU, Y., O. UNSALAN, M. AMALANATHAN, J.I. HUBERT, Infrared and Raman spectra, vibrational assignment, NBO analysis and DFT calculations of 6-aminoflavone, *J. Mol. Struct.*, 2010, **980,** 24–30, https://doi.org/10.1016/j.molstruc.2010.06.032.
9. ERIKSSON, T., S. BJÖRKMAN, B. ROTH, A. FYGE, P. HÖGLUND, Stereospecific determination, chiral inversion in vitro and pharmacokinetics in humans of the enantiomers of thalidomide., *Chirality*, 1995, **7**(1), 4452, PMID 7702998, https://doi.org/10.1002/chir.530070109.
10. FAST, P.L., J. CORCHADO, M.L. SANCHES, D.G. TRUHLAR, Optimized parameters for scaling correlation energy, *J. Phys. Chem A*. 1999, **103,** 3139–3143, https://doi.org/10.1021/jp9900382.

11. FRANCO, C.L., W.D. BERYL, J.F. PAUL, Experimental and computational approaches to estimate solubility and permeability in drug discovery and development settings, *Adv. Drug Deliv. Rev.,* 1997, **23**(1–3), 3–25, https://doi.org/10.1016/S0169-409X(96)00423-1.
12. FRISCH, A., A.B. NELSON, A. J. HOLDER, *Gauss view Molecular Visualization Program*, Gaussian Inc., Pittsburgh PA, 2001.
13. FRISCH, M.J., *et. al*. Gaussian 09; *Gaussian Inc.,* Pittsburgh, PA, 2009.
14. GADRE, S.R., I.H. SHRIVASTAVA, Shapes and sizes of molecular anions via topographical analysis of electrostatic potential, *J. Chem. Phys.,* 1991, **94**, 4384–4390, https://doi.org/10.1063/1.460625.
15. GADRE, S.R., R.K. PATHAK, Maximal and minimal characteristics of molecular electrostatic potentials, *J. Chem. Phys.*, 1990, **93**, pp. 1770–1773, ISSN: 1674-0068, http://dx.doi.org/10.1063/1.459703.
16. GEERLINGS, P., F. De PROFT, W. LANGENAEKER, Conceptual density functional theory, *Chem. Rev*., 2003, **66**(103), 1793–1874, https://doi.org/10.1021/cr990029p.
17. GONOHE, N., H. ABE, N. MIKAMI, M. ITO, Two-color photoionization of van der Waals coplexes off fluorobenzene and hydrogen-bonded complexes of phenol in supersonic jets, *J. Phys. Chem.,* 1985, **89**, 3642–3648, https://doi.org/10.1021/j100263a015.
18. GUTOWSKI, M., G. CHALASINSKI, Critical evaluation of some computational approaches to the problem of basis set superposition error, *J. Chem. Phys.,* 1993, **98**, 4540–4554, https://doi.org/10.1063/1.464901.
19. HEMMIGE, S., A. YATHIRAJAN, B. NAGARAJ, P. NAGARAJAA, D.E. LYNCH., 2,2'-Dinitrodibenzyl, *Acta Cryst.,* 2004**,** **E60**, 2455–2456, https://doi.org/10.1107/s1600536804030326.
20. JORGENSEN, W.L., E.M. DUFFY, Prediction of drug solubility from Monte Carlo simulations, *Bioorg. Med. Chem. Lett.*, 2000, **10(**11), 1155–1158, https://doi.org/10.1016/s0960-894x(00)00172-4
21. KRISHNAKUMAR, V., R.J. XAVIER, Noral coordinate analysis of 2-mercapto- and 4,6-dihydroxy-2-mercaptopyrimidines, *Indian J. Pure Appl. Phys*., 2003, **41**, 597–601, https://doi.org/10.1063/5.0109035.
22. LEE, C., W. YANG, R.G. PARR, Development of the Colle-Salvetti correlation-energy formula into a functional of the electron density. *Phys. Rev*. B, 1988, **37**, 785–789, https://doi.org/10.1103/PhysRevB.37.785.

23. LOUE, S., M. SAJATOVIC, *Encyclopedia of Women's Health*, Kluwer Academic Plenum Publishers, 2004, **J-744**, ISBN: 9780306480737.
24. MAN, H.W., L.G. CORRAL, D.I. STIRLING, G.W. MULLER, Alpha-fluoro-substituted thalidomide analogues, *Bioorganic & Medicinal Chemistry Letters.,* 2024, **13**(20), PMID 14505639, 3415–3417, https://doi.org/10.1016/S0960-894X(03)00778-9.
25. MILLER, M.T., Thalidomide embryopathy: a model for the study of congenital incomitant horizontal strabismus, *Transactions of the American Ophthalmological Society,* 1991, **89**, 623–674, PMCID: PMC1298636, PMID: 1808819.
26. NARAYAN, V., A.K. PANDEY, A. DWIVEDI , B.S. MWANKEMWA, A. MAURYA, A.K. SHARMA, V. SINGH, Comprehensive quantum chemical calculations and molecular docking analysis of uracil mustard by first principle, *Journal of the Indian Chemical Society*, 2022, **99**(8), 10058, https://doi.org/10.1016/j.jics.2022.100580.
27. PANDEY, A.K., A.K. SHARMA, S. SHUKLA, A. MISHRA, V. SINGH, A. DWIVEDI, Molecular docking, QTAIM analysis, UV-Vis spectra, vibrational analysis, and electronic properties of lantadenes C and D-A complete comparative study, *International Journal of Computational Materials Science and Engineering,* 2024, **13**(3), 2350028, https://doi.org/10.1142/S2047684123500288.
28. PANDEY, A.K., S. SHUKLA, O.P. YADAV, V. SINGH, A. DWIVEDI, A comparative vibrational analysis, electronic properties, and molecular docking of lantadene A and B (potential anticancer agents) – A computational DFT study, *J.M.C. Society,* 2024**,** **68**(3), https://doi.org/10.29356/jmcs.v68i3.2060.
29. PARR, R.G., R.A. DONNELLY, M. LEVY, W.E. PALKE, Electronegativity: The density functional viewpoint**.** *J. Chem. Phys.,* 1978, **68**, 3801–3807, https://doi.org/10.1063/1.436185.
30. PARR, R.G., R.G. PEARSON, Absolute electronegativity and hardness, *Chem. Inform.,* 1991, **22**(36), https://doi.org/10.1002/chin.199136316.
31. PARR, R.G., R.G. PEARSON, Absolute hardness: Companion parameter to absolute electronegativity, *J. Am. Chem. Soc.,* 1983, **105**, 7512–7516, https://doi.org/10.1021/ja00364a005.
32. PEARSON, R.G., Absolute electronegativity and hardness: applications to organic chemistry, *J. Org. Chem.,* 1989, **54**, 1423–1430, http://dx.doi.org/10.1021/jo00267a034.
33. POIRIER, D., Inhibitors of 17 β-hydroxysteroid dehydrogenases, *Curr. Med. Chem*., 2003, **10**(6), 453–477, https://doi.org/10.2174/0929867033368222.

34. PULAY, P., G. FOGARASI, F. PANG, J.E. BOGGS, Systematic *ab initio* gradient calculation of molecular geometries, force constants, and dipole moment derivatives, *J. Am. Chem. Soc*., 1979, **101**, 2550–2560, https://doi.org/10.1021/ja00504a009.
35. RAWAT, P., A. KUMAR, V. BABOO, R.N. SINGH, D. VERMA, D. SEXANA, H.M. GAUNIYAL, A.K. PANDEY, H. PAL, A combined experimental and quantum chemical studies on molecular structure, spectral properties, intra- and intermolecular interactions and first hyperpolarizability of 4-(Benzyloxy) benzaldehyde thiosemicarbazone and its dimer, *Journal of Molecular Structure,* 2013, **1034**, 374–385, http://dx.doi.org/10.1016/j.molstruc.2012.09.061.
36. SUBASHCHANDRABOSE, S., H. SALEEM, Y. ERDOGDU, G. RAJARAJAN, V. THANIKACHALAM, FT-Raman, FT-IR spectra and total energy distribution of 3-pentyl-2,6-diphenylpiperidin-4-one: DFT method, *Spectrochim. Acta Part A*, 2011, **82**, 260–269, https://doi.org/10.1016/j.saa.2011.07.046.
37. TEO, S.K., W.A. COLBURN, W.G. TRACEWELL, K.A. KOOK, D.I. STIRLING, M.S. JAWORSKY, Clinical pharmacokinetics of thalidomide, *Clinical Pharmacokinetics*, 2024, **43**(5), 311–327, PMID 15080764, S2CID 37728304, https://doi.org/10.2165/00003088-200443050 00004.
38. TETKO, I.V., V.Y. TANCHUK, T.N. KASHEVA, A.E. VILLA, Estimation of aqueous solubility of chemical compounds using E-state indices, *J. Chem. Inf. Comput. Sci*., 2001, **41,** 1488–93. https://doi.org/10.1021/ci000392t.
39. TETKO, I.V., V.Y. TANCHUK, T.N. KASHEVA, A.E. VILLA, Prediction of n-octanol/water partition coefficients from PHYSPROP database using artificial neural networks and E-state indices, *J. Chem. Inf. Comput. Sci.,* 2001, **41**, 1407–1421, https://doi.org/10.1021/ci010368v.
40. TOLLET, P., M. HAMBERG, J.A. GUSTAFSSON, A. MODE, Growth hormone signaling leading to *CYP2C12* gene expression in rat hepatocytes involves phospholipase A2, *Journal of Biological Chemistry*, 1995, **270**(21), 12569−12577, PMID: 7759504 https://doi.org/10.1074/jbc.270.21.12569.
41. VERMA, R.P., C. HANSCH, A comparison between two polarizability parameters in chemical-biological interactions, *Bioorg. Med. Chem.,* 2005, **13**, 2355–2372, https://doi.org/10.1016/j.bmc.2005.01.051.
42. VERMA, R.P., A. KURUP, C. HANSCH, On the role of polarizability in QSAR, *Bioorg. Med. Chem.,* 2005, **13**, 237–255, https://doi.org/10.1016/j.bmc.2004.09.039.

43. VIRGILIO, F.D., L.-H. JIANG, S. ROGER, S. FALZONI, A.C. SARTI, V. VULTAGGIO-POMA, P. CHIOZZI, E. ADINOLFI, Structure, function and techniques of investigation of the P2X7 receptor (P2X7R) in mammalian cells, *Methods in Enzymology*, 2019, **629**, 115–150, https://doi.org/10.1016/bs.mie.2019.07.043.
44. YANG, W., W.J. MORTIER, The use of global and local molecular parameters for the analysis of the gas-phase basicity of amines, *J. Am. Chem. Soc.,* 1986, **108**, 5708–5711, https://doi.org/10.1021/ja00279a008.
45. ***BRITISH NATIONAL FORMULARY (BNF editing committee) 76 (76 ed.), *Pharmaceutical Press*, 2018, p. 936, ISBN-13: 978-0857113382.
46. ***https://www.rcsb.org/
47. ***Thalidomide C13H10N2O4. *Pub. Chem., National Library of Medicine*, CID 5426, 2023, https://pubchem.ncbi.nlm.nih.gov/compound/Thalidomide.
48. ***Thalidomide Celgene 50 mg Hard Capsules – Summary of Product Characteristics., *UK Electronic Medicines Compendium.*, January 2017, MAM: EU/1/08/443/001. https://ec.europa.eu/health/documents/community-register/2018/20180208139808/anx_139808_en.pdf.
49. ***Thalidomide Monograph for Professionals., *Drugs.com.* 10 Nov. 2024. https://www.drugs.com/monograph/thalidomide.html.
50. ***US Thalidomide label (PDF). *FDA.,* January 2017, NDA 020785/S-063, Reference ID: 4117081, https://www.accessdata.fda.gov/drugsatfda_docs/appletter/2017/020785Orig1s063ltr.pdf
51. ***www.swissdock.ch